Frustration in a generalized kagomé Ising antiferromagnet: Exact results

K. A. Muttalib and J. H. Barry
Department of Physics, University of Florida, P.O. Box 118440, Gainesville, Florida 32611-8440, USA

(Received 24 February 2022; accepted 4 July 2022; published 29 July 2022)

We obtain the exact ground-state phase diagram of a generalized kagomé antiferromagnet with both pair and triplet interactions, J_2 and J_3, respectively, in the presence of a magnetic field h appropriately tuned. We find that when the pair interaction $J_2 < 0$ dominates, the ground state is geometrically frustrated; on the other hand, the ground state is disordered but not frustrated when the triplet interaction J_3 dominates, the boundaries between the two cases being at $J_3 = \pm J_2$. The exact ground-state crossover lines between the two distinct types of disorder remain identifiable crossover curves at finite temperatures. In the frustrated domain, the ground state of the three-parameter model is identical to the ground state of the prototype one-parameter ($J_2 < 0$) model of geometrical frustration. Towards further understanding the frustration domain of the three-parameter model, a closed-form approximation (exact at zero temperature) determines solutions on a two-parameter subspace for induced magnetization and parallel magnetic susceptibility at finite fields h and temperatures T, the inverse susceptibility showing a Curie-Weiss behavior. We argue that the existence of an exact $T = 0$ threshold magnetic field, below which the magnetization remains zero, indicates the existence of a gapped spectrum attributable to the presence of the triplet interaction J_3.

DOI: 10.1103/PhysRevE.106.014149

I. INTRODUCTION

Geometrical frustration in spin systems can lead to novel and interesting disordered phases like spin glass, spin liquids, and spin ice, including the so-called kagomé ice [1–27]. In lattice-statistical spin models, geometrical frustration traditionally stems from *antiferromagnetic* nearest-neighbor spin couplings on close-packed lattices (triangular faces). The "kagomé spin ice" model [23] deserves special attention. The three-parameter Ising model entails an applied magnetic field and both first- and second-nearest neighbor pair interactions (Ising anisotropies). The model is nonplanar (crossing interaction bonds) and thus is nonintegrable. Significantly, however, using classical simulations and Monte Carlo calculations, the kagomé spin ice results reveal *frustrated ferromagnetism*. Many approximation schemes and numerical techniques have been developed to understand the properties of various theoretical models like the spin 1/2 Heisenberg model or the asymmetric or extended Hubbard model on a geometrically frustrated lattice [28–55]. It is well known that classical Ising models with antiferromagnetic nearest-neighbor pair interactions on either the triangular or kagomé lattice in two dimensions have disordered ground states due to frustration [56–58]. On the other hand, it has recently been shown [59] that a purely triplet Ising interaction model on a kagomé lattice also leads to a highly disordered ground state but without frustration, very similar to a purely four-spin interaction model on a three-dimensional pyrochlore lattice [60]. Each of these models has a high degree of degeneracy in the ground state with finite residual entropy per site, but their magnetic properties are very different. For example, the perpendicular susceptibility $\chi_\perp$ of the kagomé Ising model with only antiferromagnetic pair interaction diverges as $T \to 0$, while $\chi_\perp$ of the triplet model remains finite. Similarly the parallel susceptibility of the pair interaction model leads to a finite Curie-Weiss temperature Θ_{CW} while $\Theta_{CW} = 0$ for the triplet model. Thus the two types of disorder are clearly distinguishable by their magnetic response. We will call the disorder with frustration as *frustrated disorder* (FD) and the disorder without frustration as *nonfrustrated disorder* (NFD). The question arises, What happens when pair and triplet interactions are mixed?

Real physical systems with kagomé lattice structure and antiferromagnetic pair interactions have been studied experimentally [61–64]. While dominant triplet interactions are not ubiquitous in real systems, they can nevertheless be present as a perturbation to a dominant pair interaction, e.g., in the description of fluids in the critical region or magnetism in solid He^3 with multiparticle ring exchange [65–68]. They also arise as part of multispin interactions describing effective models of alloys and spin-glass models [69–72]. A model combining both interactions is therefore quite realistic and can provide useful insights into the interplay of the two types of disorder mentioned above. Such interactions can also be explored in optical lattices with cold atom technology [73–75]. In the present paper, we consider a kagomé Ising model with both antiferromagnetic pair ($J_2 < 0$) and localized triplet interactions (J_3), together with an external magnetic field (h), generalizing the standard two-parameter kagomé Ising antiferromagnet.

A generalized model with *ferromagnetic* pair interaction ($J_2 > 0$) was recently investigated to determine the complete zero-temperature phase diagram by tuning the magnetic field appropriately [76]. It was found that while long-range order exists for ferromagnetic pair interactions, this order is destroyed by sufficiently large (positive or negative) triplet interaction. In the J_2-J_3 plane, the ferromagnetic-paramagnetic boundary occurs at $|J_3| = 3J_2$. In this paper, we analyze the model with *antiferromagnetic* pair interaction ($J_2 < 0$) in which case there is no long-range ordering for any values of the parameters. The three-parameter kagomé model is mapped on to a two-parameter honeycomb Ising model with a field L^* and pair interaction K^*, but no triplet interaction. We show that this model is exactly solvable under the condition $L^* = 0$, which is an exact solution of the original three-parameter kagomé model on a two-parameter subspace.

In the limit $T \to 0$ and within the subspace, the above mapping allows us to first obtain the ground-state phase diagram *exactly* and show that both types of disorder (FD and NFD) exist, with a clear boundary between them at $|J_3| = -J_2$ in the J_2-J_3 plane. The region where pair interaction dominates belongs to FD, while the triplet-interaction-dominated region is NFD, both consistent with the special cases considered in [59]. The boundary between FD and NFD at zero temperature occurs where the strength of the triplet interaction is equal to that of the pair interaction. This implies that for most materials where J_3 is expected to be much smaller than J_2, this boundary will not be accessible experimentally. However, we also show that at finite temperature this boundary depends on the ratio $|J_3/J_2|$. We obtain this crossover temperature, which increases with decreasing $|J_3|$ for a given $|J_2|$. We therefore argue that for realistic materials, the boundary can be probed experimentally at a sufficiently high temperature.

It develops that it is also possible to obtain the induced magnetization as well as the parallel magnetic susceptibility as a function of the field or the temperature in the aforementioned two-parameter subspace. The susceptibility as a function of temperature T diverges as $1/(T + T_0)$, with T_0 a positive constant, as expected for an antiferromagnet; this allows for an estimate of the Curie-Weiss temperature Θ_{CW}. As $J_3 \to 0$, this value tends to the kagomé Ising antiferromagnet $\Theta_{CW}^{KIA} = 4|J_2|/k_B$, with k_B being the Boltzmann constant. The existence of a threshold field before the magnetization starts to rise with increasing field implies the existence of a gapped spectrum due to the triplet interaction J_3.

The exact solutions use the equivalence of the canonical partition functions of a three-parameter generalized kagomé Ising magnet and a standard two-parameter Ising magnet on an associated honeycomb lattice, with the grand canonical partition function of a generalized three-parameter kagomé lattice gas having a direct connection [76]. The solution proceeds by solving the phase boundary of the lattice-gas model first (although it lacks a physical fluid meaning in the frustrated regime) and then obtaining the magnetic solutions by using generalized fluid-magnet correspondence relations.

In these theoretical investigations of geometrical frustration, all ground-state results for the three-parameter model are exact. The results include, e.g., the ground-state phase diagram and the threshold magnetic fields attributable to the presence of the triplet interaction J_3. The investigations also determine the crossover curve at *finite* temperatures separating the FD and NFD disordered regions. Moreover, in the frustrated (FD) region, the ground state of the generalized (three-parameter) model is identical to the ground state of the standard 1-parameter ($J_2 < 0$) model (all elementary triangles are frustrated at $T = 0$ in both models) implying that all ground-state results known for the prototype model are transferable to the current generalized model such as residual entropy [58] and $T = 0$ localized correlations [77].

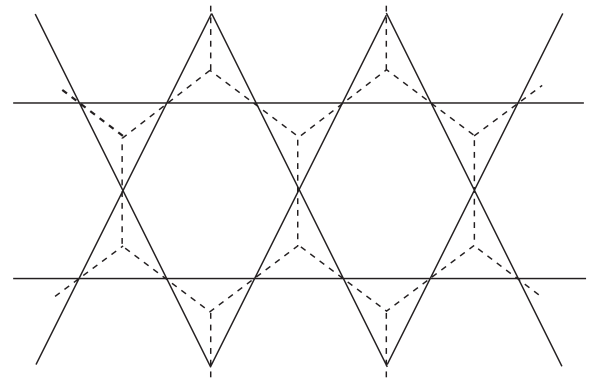

FIG. 1. A kagomé lattice (solid edges) and its associated honeycomb lattice (dashed edges).

The remainder of the paper is organized as follows. In Sec. II we introduce the model and in Sec. III we outline the formal mappings that provide the background and notations for our current exact results. These mappings were already discussed and used in [76], so we only summarize them briefly. In Sec. IV we use the mappings to identify two types of disorder FD and NFD and obtain the boundary between them. In Sec. V we focus on the frustrated region and obtain exact solutions for the ground state as well as induced magnetization and parallel magnetic susceptibility of the three-parameter model on a two-parameter subspace. In Sec. VI we explore the possibility of going beyond the two-parameter subspace within a perturbative approach. We summarize our results in Sec. VII. Appendix A contains a direct proof that the magnetic field parameter L^* in the associated honeycomb Ising antiferromagnet is pure imaginary if the ground state is geometrically frustrated, while Appendix B proves that all zero-field odd-number correlations vanish identically in the ground state ($T = 0$) for such frustrated domains. In Appendix C we obtain the condition for $L^* = 0$ in the FD region in the limit $T \to 0$. Appendix D obtains the zero-temperature limits $L^*(T \to 0)$ in the FD and NFD regions.

II. THE GENERALIZED KAGOMÉ ISING ANTIFERROMAGNET

In [59] a pair and a triplet Hamiltonian were considered separately,

$$-H_{pair} = J_2 \sum_{<i,j>} \sigma_i\sigma_j, \tag{2.1a}$$

$$-H_{triplet} = J_3 \sum_{<i,j,k>} \sigma_i\sigma_j\sigma_k, \tag{2.1b}$$

where $\sigma_l = \pm 1,\ l = 0, 1, \ldots, \mathcal{N} - 1$ are the Ising variables ($\mathcal{N}$ being the total number of sites of a kagomé lattice), the summation $\sum_{<i,j>}$ is taken over all distinct nearest-neighbor pairs of sites of a kagomé lattice (see Fig. 1, solid edges), and $\sum_{<i,j,k>}$ is taken over all triplets of sites belonging to elementary triangles. Both models were shown to have disordered ground states for $J_2 < 0$ and arbitrary J_3. Here we add a magnetic field and consider the combined Hamiltonian

$$-H_I = h\sum_i \sigma_i + J_2 \sum_{<i,j>} \sigma_i\sigma_j + J_3 \sum_{<i,j,k>} \sigma_i\sigma_j\sigma_k. \quad (2.2)$$

The inclusion of a longitudinal magnetic field h enables investigations of $\chi_{\parallel}$, the parallel magnetic susceptibility of the model. We will call model (2.2) a *generalized kagomé antiferromagnet*.

The partition function for model (2.2) can be mapped exactly, via an intermediate lattice-gas model in the grand canonical ensemble, to the partition function of a standard Ising model on an associated honeycomb lattice (see Fig. 1, dashed edges) with a magnetic field and a nearest-neighbor pair interaction without any triplet interaction. Using this mapping, (2.2) with ferromagnetic pair interaction was solved exactly for the zero-temperature phase diagram with long-range order [76]. Here we will consider antiferromagnetic pair interactions and study the regions where there is no long-range ordering. In order to introduce the background and appropriate notations, we give here a brief outline of the mapping. For details we refer to [76].

III. MAPPINGS

The mappings outlined in [76] are done in two parts. The first part establishes the equivalence between the magnetic canonical partition function of (2.2) with the grand canonical partition function of a generalized kagomé lattice-gas model

$$-H_{lg} = \epsilon_2 \sum_{<i,j>} n_i n_j + \epsilon_3 \sum_{<i,j,k>} n_i n_j n_k, \quad (3.1)$$

where ϵ_2, ϵ_3 are pair and triplet interaction parameters, respectively. The lattice-gas variables n_l are idempotent site-occupation numbers defined as $n_l = 1$ if site l is occupied and 0 if site l is empty. In (3.1), an infinitely strong (hard-core) repulsive pair potential has also been tacitly assumed for atoms on the *same* site, thereby preventing multiple occupancy of any site as reflected in the dichotomic values of the occupation numbers. Defining

$$L \equiv \beta h, \quad K \equiv \beta J_2, \quad M \equiv \beta J_3 \quad (3.2)$$

and

$$K_2 \equiv \beta\epsilon_2, \quad K_3 \equiv \beta\epsilon_3 \quad (3.3)$$

with $\beta \equiv 1/k_B T$ being the "inverse temperature," the equivalence is given as

$$e^{(L-2K+2M/3)\mathcal{N}} Z(L,K,M) = \Xi(\mu,\mathcal{N},T), \quad (3.4)$$

with

$$L = K_2 + \frac{K_3}{4} + \frac{\beta\mu}{2}, \quad K = \frac{K_2}{4} + \frac{K_3}{8}, \quad M = \frac{K_3}{8}. \quad (3.5)$$

Here [in (3.4)] the magnetic canonical partition function $Z(L,K,M)$ associated with (2.2) is given by

$$Z(L,K,M) \equiv Tr_\sigma e^{-\beta H_I}, \quad (3.6)$$

and the grand partition function $\Xi(\mu,\mathcal{N},T)$ associated with (3.1) is given by

$$\Xi(\mu,\mathcal{N},T) \equiv Tr_n e^{-\beta(H_{lg}-\mu N)}, \quad (3.7)$$

where μ is the chemical potential with N being the conjugate total number of particles, $N = \sum_i n_i$, $i = 0,1,\ldots,\mathcal{N}-1$. For later purposes, we define

$$x \equiv e^{K_2}, \quad y \equiv e^{K_3}, \quad z \equiv e^{\beta\mu} \quad \text{(fugacity)}. \quad (3.8)$$

The relations (3.5) between the parameters of the generalized magnet (3.6) and the generalized fluid (3.7) effectuate a generalized fluid-magnet correspondence. The one-to-one mapping between fluid and magnetic phase boundaries is direct and valuable. More definitely, we define the parameters α and α' as

$$\alpha \equiv -\frac{\epsilon_3}{\epsilon_2}, \quad \alpha' \equiv -\frac{J_3}{J_2}. \quad (3.9)$$

Using (3.3) and (3.8), this implies

$$y = x^{-\alpha}. \quad (3.10)$$

In addition, (3.2), (3.3), (3.5), and (3.9) can be combined to obtain the fluid-magnet correspondence relation

$$\frac{h}{J_2} = \frac{4}{2-\alpha}\left(\frac{\mu}{\epsilon_2} + \frac{4-\alpha}{2}\right). \quad (3.11)$$

The relation between α and α' turns out to be simply given by

$$\alpha' = \frac{\alpha}{2-\alpha}. \quad (3.12)$$

In the second part, a mapping establishes the equivalence (aside from known prefactors) between the grand canonical partition function $\Xi(\mu,\mathcal{N},T)$ of a generalized lattice-gas model on the kagomé lattice with a standard two-parameter Ising antiferromagnet on the associated honeycomb lattice (Fig. 1 with dashed edges)

$$-\beta H^*_{hc} = L^* \sum_i \mu_i + K^* \sum_{<ij>} \mu_i\mu_j, \quad (3.13)$$

where each site-localized Ising variable $\mu_l = \pm 1$, $l = 1,\ldots,\mathcal{N}^*(= 2\mathcal{N}/3)$, and L^*, K^* are dimensionless parameters for the magnetic field and nearest-neighbor pair interaction, respectively.

The equivalence is given by

$$\Xi(\mu,\mathcal{N},T) = Z_{8V}(a,b,c,d) = (a^*/2\cosh L^*)^{\mathcal{N}^*} \times (1/\cosh K^*)^{\frac{3\mathcal{N}^*}{2}} Z^*(L^*,K^*). \quad (3.14)$$

Here the magnetic canonical partition function of the model (3.13) is given by

$$Z^*(L^*,K^*) = Tr_\mu e^{-\beta H^*_{hc}}, \quad (3.15)$$

where the trace symbol μ represents the set of total $\mathcal{N}^*$ Ising variables [no confusion with the chemical potential in (3.7) should arise]. The parameters K^*, L^*, and a^* are given in terms of the vertex weights of the intermediate honeycomb symmetric eight-vertex model partition function $Z_{8V}(a,b,c,d)$ (see Appendix A).

We emphasize at this point, for later interpretations, that while the field L^* is real for $K^* > 0$, the mapping guarantees that it is *pure imaginary* for $K^* < 0$. This might seem puzzling, since it makes the Hamiltonian (3.13) non-Hermitian. However, (3.13) is $\mathcal{PT}$ symmetric, where $\mathcal{P}$ and $\mathcal{T}$ refer to parity and time-reversal symmetry, respectively, guaranteeing real eigenvalues [78]. The important point to keep in mind is that the mapping is between partition functions, and the partition function (3.15) corresponding to (3.13) remains real and physical when L^* is pure imaginary, as shown in Appendix B. Concerning the condition $L^* = 0$, one is reminded that the (3.15) partition function $Z^*(L^*, K^*)$, $L^* \neq 0$, of a standard form planar Ising model (3.13) persists as arguably the most noted *unsolved* partition function in statistical mechanics! In the present work, we will mostly consider the case $L^* = 0$, for which the Hamiltonian (3.13) is Hermitian.

The pair-interaction parameter K^* plays a key role in the current theory and can be rewritten [76] in terms of the lattice-gas parameters x, y, z as

$$4K^* = \ln\left\{1 + \frac{x^2zl}{[x^2z(xy-1)+x-1]^2}\right\}, \tag{3.16}$$

where

$$l = l(x, y) \equiv (x^2y-1)^2 - 4(x-1)(xy-1). \tag{3.17}$$

The null (or nodal) condition $l = 0$ separates the ferromagnetic ($K^* > 0$) and antiferromagnetic ($K^* < 0$) disordered regions in (3.16). The general expressions for a^* and L^* in (3.14) are complicated, and we write the complete expressions in Appendix A.

IV. TWO TYPES OF DISORDER

The generalized kagomé antiferromagnet model (2.2) with $J_2 < 0$ has states that remain disordered down to zero temperature for all values of the parameters, as shown in [76]. We show below how a detailed study of the parameter K^* in (3.16) allows us to identify two distinct types of disorder that separate the J_2-J_3 space with a clear boundary between them.

A. The parameter K^*

As a result of the mapping from a three-parameter kagomé Ising antiferromagnet (2.2) to a two-parameter honeycomb Ising model (3.13), K^* in (3.13) is not a standard reduced (dimensionless) pair-interaction parameter; it is a highly nontrivial function of all of the parameters of (2.2). The expression (3.16) for K^* is in terms of the intermediate lattice-gas parameters, related to the parameters of (2.2) by the fluid-magnet correspondence relation (3.11). Clearly, given (3.16), different zero-temperature limits of K^* exist for different choices of the parameter $\alpha = -\epsilon_3/\epsilon_2$. These limits determine whether the corresponding ground state is ordered or disordered. In particular, under a *zero field condition* $L^* = 0$, it is known [79] that the ground state of (3.13) has a sublattice long-range ferromagnetic order if $K^*(T \to 0) > K_c^*$, where K_c^* is a known critical value

$$K_c^* = \frac{1}{2}\ln(2+\sqrt{3}). \tag{4.1}$$

The system remains disordered down to zero temperature if $K^* < K_c^*$.

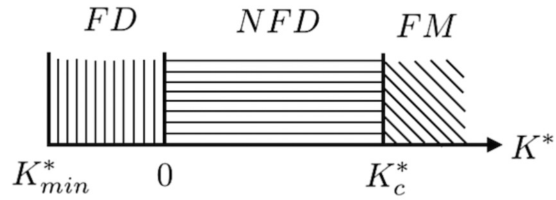

FIG. 2. Schematic. Range of K^* in (3.16) corresponding to different ordered and disordered regions, with $K_c^* = \frac{1}{2}\ln(2+\sqrt{3}) = 0.6584\ldots$ and $K^*_{min} = -\frac{1}{2}\ln 2 = -0.3465\ldots$. FM refers to the ferromagnetic ordered region. FD and NFD correspond to frustrated and nonfrustrated disorder, respectively.

In order to study the nature of the disordered state, we recall that a model of Ising spins with dimensionless pair interactions K^* on a honeycomb lattice (and zero field) can be mapped on to a model of Ising spins with zero field and a dimensionless pair interaction $K = \beta J_2$ on a kagomé lattice, given by [77]

$$e^{4\beta J_2} = 2e^{K^*} - 1. \tag{4.2}$$

For $K^* > 0$, the right-hand side is greater than 1, and so J_2 must be positive. This implies that the mapping is on to a model of Ising spins on the kagomé lattice with *ferromagnetic* interactions. Note that K_c^* defines a critical temperature in the kagomé lattice model given by $e^{4\beta_c J_2} = 2e^{K_c^*} - 1$. For $0 < K^* < K_c^*$, $T > T_c$ and the mapping is on to a kagomé lattice ferromagnetic pair interaction model at a temperature higher than the critical temperature. Thus the disorder is not related to any geometric frustration. As shown in [59], geometric frustration leads to the perpendicular susceptibility $\chi_\perp$ diverging as $1/T$ near zero temperature; the parameter $\eta_0 \propto \lim_{T\to 0}[T\chi_\perp(T)]$ gives a measure of the degree of frustration. For example, the kagomé triplet interaction model $H_{triplet} = -J_3\sum_\tau \sigma_i\sigma_j\sigma_k$, $J_3 < 0$ and τ corresponding to all elementary triangles in a kagomé lattice is clearly not geometrically frustrated but still highly disordered with a large residual entropy, consistent with $\eta_0 = 0$. Note that η_0 is also zero for kagomé Ising model with nearest-neighbor ferromagnetic interactions, which has long-range order below a critical temperature. Above the critical temperature the system is disordered, and this is clearly not due to geometrical frustration.

On the other hand, for $K^* < 0$, (4.2) shows that J_2 must be negative. Thus the mapping is on to a model of Ising spins on the kagomé lattice with *antiferromagnetic* interactions. Disorder in this case is related to geometrical frustration (with finite η_0) since the kagomé lattice contains elementary triangles. Note that the transformation (4.2) limits the range of K^*; namely, the minimum value is given by

$$K^*_{min} = -\frac{1}{2}\ln 2, \tag{4.3}$$

which corresponds to $\beta J_2 \to -\infty$.

Thus the parameter K^* in (3.13) can range from K^*_{min} to values larger than K_c^*, depending on the parameter α. Figure 2 shows different ranges of K^* as described above. For the sake of completeness, the range $-\infty < K^* < K_N^*$ relates to an ordered antiferromagnetic Néel state, where the zero field

$K_N^*(=-K_c^*)$ is a Néel critical value. This range is safely below the current range of interest for K^*, *viz.*, $K_N^* < K_{min}^*$ in Fig. 2.

B. Zero-temperature phase diagram

As was done for the ordered vs disordered domains, analysis of the zero-temperature limits of (3.16) under the $L^* = 0$ condition allows one to obtain the boundary between the two types of disordered regions, with and without frustration. In the mappings of Sec. III, the Ising parameter K^* is a function of the lattice-gas parameters x, y and z. Therefore it will be easier to consider the ground-state phase diagram of the lattice-gas model in the ϵ_2-ϵ_3 plane first and then transform it to the J_2-J_3 plane using the fluid-magnet correspondence. This strategy was followed in Ref. [76], where it was found that in the ground state, the lines $\alpha = 1.5$ and $\alpha = 3$ separate the ordered from the disordered regions in the ϵ_2-ϵ_3 plane as shown in Fig. 3(a). In the corresponding magnetic phase diagram, the lines $\alpha' = \pm 3$ separate the ordered from the disordered regions in the J_2-J_3 plane, as shown in Fig. 3(b). Also, the ground-state (reduced) magnetic field $h/2|J_2|$ can be conjoined with the frustrated disordered region in Fig. 3(b). Using the (3.9) definition $\alpha' \equiv -J_3/J_2$ and (4.4), the conjunction is easily established *above* the $J_2 < 0$ axis (second quadrant) to be $h/2|J_2| = \alpha'$, $0 < \alpha' < 1$ $(h > 0)$, and *below* the $J_2 < 0$ axis (third quadrant) as $h/2|J_2| = \alpha'$, $-1 < \alpha' < 0$ $(h < 0)$. We should emphasize that, unlike the ferromagnetic case, the corresponding lattice-gas model lacks any physical interpretation in the frustrated regime, but is used solely as a mathematical tool.

Given that all of the first quadrant plus the region $\alpha > 3$ in the second quadrant in Fig. 3(a) is ordered, we start by considering the region $\alpha \leqslant 3$ in the second quadrant, where $\epsilon_2 < 0$ and $\epsilon_3 > 0$. In this case, the zero-temperature limit corresponds to $x \to 0$.

The present work is based on the recognition that the disordered phase in the region $0 < \alpha < 3$ can again be separated into two distinct regions. Below we consider the two regions separately, characterized by $1 < \alpha < 3$ and $0 < \alpha < 1$. We will show that $K^*(T \to 0)$ is positive for $1 < \alpha < 3$, while it is negative for $0 < \alpha < 1$. This implies that the $\alpha = 1$ line in the $\epsilon_2 - \epsilon_3$ plane separates frustrated disorder (FD) from nonfrustrated disorder (NFD) in the J_2-J_3 plane.

Case I: $1 < \alpha < 3$

For $1 < \alpha < 3$, the quantity l given by (3.17) has the dominant diverging term $l \sim 4x^{1-\alpha}$ as $x \to 0$. This implies that $l > 0$, and therefore, using (3.16), $K^*(T \to 0)$ is positive. Note that in this case there is no physical solution satisfying the null condition $L^* = 0$, since the existence of such a solution would imply a long-range order. However, as long as $K^* < K_c^*$, the field L^* goes to zero in the limit $T \to 0$, as can be seen from the zero-temperature limit of (A5), obtained in (D2). Thus the ground state is disordered but without frustration, or NFD.

Case II: $0 < \alpha < 1$

On the other hand, for $0 < \alpha < 1$, the dominant term for l at zero temperature is $l \to -3$. It then follows that $K^*(T \to 0)$ is negative, and therefore J_2 is also negative. The null

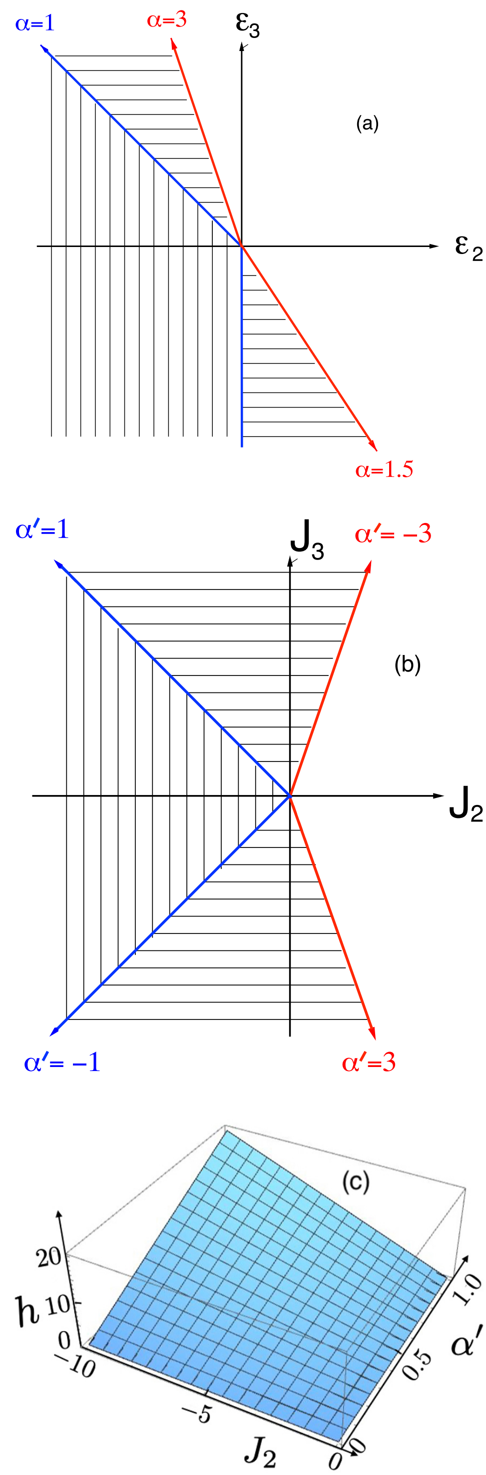

FIG. 3. Zero-temperature exact phase diagrams of (a) the lattice-gas model, (b) the magnet model, and (c) the vertically dashed region of (b) for $\alpha' > 0$, including the field h. In (a) and (b), the ordered regions are unshaded, as obtained in Ref. [76]; the red lines separate the ordered from the disordered regions. The nonfrustrated disordered (NFD) regions are shaded by horizontal lines and are characterized by $0 < K^* < K_c^*$. The frustrated disordered (FD) region $K_{min}^* \leqslant K^* < 0$ is shaded by vertical lines. Established later is the relation $h = 2J_3$ in the vertically lined FD region of 3(b). The blue lines separate the two distinct types of disordered regions. In (c), the conditions $h = 2J_3$ and $L^* = 0$ are satisfied everywhere on the ground-state (blue) surface.

condition $L^* = 0$ in this case is not a condition for long-range order as in a ferromagnet [76], but provides a solution of the model on a two-parameter subspace since it provides a relationship among the three parameters x, y, and z. At zero temperature, as shown in (C8), this is given by

$$\frac{h}{2J_3} = 1, \quad T \to 0. \tag{4.4}$$

Thus, in the ground state, the $L^* = 0$ condition is equivalent to the condition $h = 2J_3$. The condition also implies $K^* = K^*_{min}$ (see Sec. VI), and this in turn implies that $\beta J_2 \to -\infty$. This is true for either $T \to 0$ and finite J_2 or $J_2 \to -\infty$ and finite temperature. In either case, the ground state is disordered due to frustration.

Using the fluid-magnet correspondence relations (3.11) and (3.12), we see that for $J_2 < 0$ and in terms of the parameter $\alpha' = -J_3/J_2$, the regime $0 < \alpha' < 1$ corresponds to frustrated disorder, while the regime $\alpha' > 1$ corresponds to nonfrustrated disorder:

$$\begin{aligned} 0 < K^* < K^*_c, &\quad \alpha' > 1: \text{ NFD} \\ K^*_{min} < K^* < 0, &\quad \alpha' < 1: \text{ FD}, \end{aligned} \tag{4.5}$$

where FD denotes frustrated disorder and NFD denotes nonfrustrated disorder.

Mathematically, the difference between disorder with and without frustration manifests itself also in the corresponding magnetic field L^* in (3.13), which is real for $K^* > 0$ but is pure imaginary for $K^* < 0$. The fact that L^* is pure imaginary for $K^* < 0$ is known from the Wu theory [80], but it can also be seen directly from the expression of L^* given by (A5) in Appendix A. This in turn affects the spin correlations and therefore the magnetic response in the two cases. In particular, when L^* is pure imaginary, we show in Appendix B that all zero-field odd-number correlations must vanish at zero temperature in the associated honeycomb Ising model with its even-number interactions.

Thus the line $\alpha' = 1$ separates the two types of disorder in the second quadrant of Fig. 3(b). Moreover, using the intrinsic symmetry of the magnetic canonical partition function $Z(h, J_2, J_3) = Z(-h, J_2, -J_3)$, this implies that the line $\alpha' = -1$ in the J_2-J_3 plane also separates the two types of disorder in the third quadrant. Mapping back to the lattice-gas model, this implies that the line $\alpha \to \infty$, i.e., the line separating the third and the fourth quadrants, corresponds to the boundary between the two types of disorder. In other words, the entire third quadrant in the ϵ_2-ϵ_3 plane corresponds to $K^* < 0$. Thus the above analysis leads to the partitioning shown in Figs. 3(a) and 3(b). In addition, the ground state in the FD region corresponds to $h = 2J_3$; Fig. 3(c) shows a 3D plot in the restricted region $J_2 < 0$ and $0 < \alpha' < 1$, with h added as a third axis.

We note that according to Fig. 3(b), the limiting case of H_{pair} in (II.1 a) with $J_3 = 0$ and $J_2 < 0$ is an example of disorder due to frustration, while the limiting case of $H_{triplet}$ in (II.1 b) with $J_2 = 0$ belongs to nonfrustrated disorder. As shown in Ref. [59], the magnetic properties of these two limiting cases are very different. In particular, the perpendicular susceptibility diverges for the frustrated system while it remains finite in the case of nonfrustrated disorder. Also, the mean-field Curie-Weiss temperature is finite for the frustrated model, while it is zero for nonfrustrated disorder. Moreover, as shown in Appendix B, all zero-field odd-number correlations vanish at zero temperature in the geometrically frustrated region of the associated honeycomb Ising model. Thus the two types of disordered states have very different magnetic responses that should be experimentally observable.

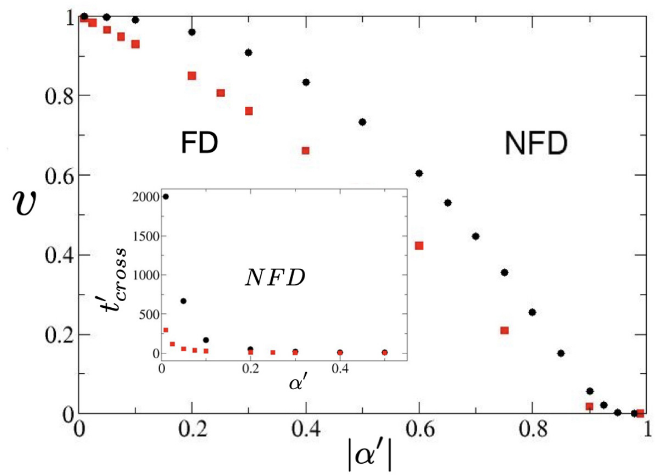

FIG. 4. Exact solution for the crossover temperature T_{cross} (black dots), obtained from numerical solution of (4.7) between frustrated disorder FD and nonfrustrated disorder NFD, ranges from 0 to ∞ as $v \equiv e^{-4|J_2|/k_B T_{\text{cross}}}$ ranges from 0 to 1. The red squares show the $K^* = 0$ curve under the condition $L^* = 0$. Here $\alpha' \equiv -J_3/J_2$ and $t'_{\text{cross}} = k_B T_{\text{cross}}/2|J_2|$

C. Crossover at finite temperature

As mentioned before, the condition $K^* = 0$ separates the FD from NFD regime. From (3.16) and (3.17), K^* is zero when $l = 0$. We define

$$v \equiv [e^{-\frac{|\epsilon_2|}{k_B T_{\text{cross}}}}]^{\frac{1}{1+\alpha'}} = e^{-\frac{4|J_2|}{k_B T_{\text{cross}}}}, \tag{4.6}$$

where we used the relations (3.3) and (3.5) [see also (6.4)] to obtain the second equality. In terms of v, using (3.17), the condition $l = 0$ is given by

$$(1 - v)^3(3 + v) = 16v \sinh^2\left(\frac{\alpha'}{2} \ln v\right). \tag{4.7}$$

Numerical solution of this equation is shown in Fig. 4, the inset showing $t'_{\text{cross}} \equiv k_B T_{\text{cross}}/2|J_2|$. The black dots represent a crossover boundary between $K^* < 0$ and $K^* > 0$, or between FD and NFD. Observationally, this crossover temperature is too high for small values of α', although it should be experimentally accessible for values of α' close to 1.

We mention here that in the rest of the paper we will consider exact results for magnetization and magnetic susceptibility, but only under the condition $L^* = 0$. Under this condition, K^* becomes zero at a crossover temperature, which is always smaller than the true crossover temperature obtained from the $l = 0$ condition. Therefore, it has a limiting effect on our ability to study the true crossover region. Because it plays an important role in the limitation of our calculation, we show the $L^* = 0$ boundary in Fig. 4, with red squares. For example, for $\alpha' = 0.01$, the actual crossover temperature is close to $t'_{\text{cross}} = 2000$, while it is only about 300 within the $L^* = 0$ subspace as shown in the inset of Fig. 4. Thus, as we will see later, the inverse susceptibility under the $L^* = 0$ condition will diverge at the boundary determined by the red squares, leaving us with no information near the true crossover boundary (the black dots), except near $\alpha' = 0$ or 1 where the two crossover temperatures coincide.

V. FRUSTRATED DISORDER IN THE $L^* = 0$ SUBSPACE

As shown in Appendix C, the condition $L^* = 0$ defines a two-parameter subspace in the grand canonical fluid model (3.1) with three parameters $x = e^{\beta\epsilon_2}$, $y = e^{\beta\epsilon_3}$, and $z = e^{\beta\mu}$, where μ is the chemical potential. Using the fluid-magnet correspondence relations (3.11), this defines a two-parameter subspace in the three-parameter h, J_2, and J_3 space of the canonical magnetic model (2.2). Many interesting physically observable results, like the finite-temperature results for magnetization and magnetic susceptibility, can be obtained exactly in this subspace. The caveat is that the magnetic field h is no longer an independent parameter, but must be tuned to guarantee the $L^* = 0$ condition.

A. Ground-state properties

From Appendix C, Eq. (C8), $h \to 2J_3$, as $T \to 0$. Thus in the ground state, the $L^* = 0$ condition is equivalent to the condition $h = 2J_3$. Moreover, the $L^* = 0$ condition at zero temperature secures the minimum of K^*, as shown in Fig. 14 for $\theta = 0$. Combining the above results, we find that for the limit $T \to 0$, the $L^* = 0$ condition is equivalent to $h = 2J_3$ and $K^* = -(1/2)\ln 2$. In other words, if we start with a generalized kagomé Ising model

$$-H_k = 2J_3 \sum_i \sigma_i - |J_2| \sum_{<i,j>} \sigma_i\sigma_j + J_3 \sum_{<i,j,k>} \sigma_i\sigma_j\sigma_k, \quad (5.1)$$

where we tuned the field h to be exactly equal to $2J_3$, then the ground-state properties can be obtained from the standard Ising model on the associated honeycomb lattice with zero field,

$$-\beta H^*_{hc} = -\frac{1}{2}\ln 2 \sum_{<i,j>} \mu_i\mu_j. \quad (5.2)$$

The following simple considerations provide additional insights into the $L^* = 0$ subspace. We first decompose the kagomé lattice into three (α, β, γ) sublattices. Consider a simple frustrated configuration, consisting of an entirety of frustrated elementary triangles. More pertinently, consider *every* elementary triangle in the kagomé lattice to have the *same* frustrated spin configuration shown in Fig. 5. Then the magnetic and the triplet interaction terms in (2.2) together can be calculated to give the Zeeman plus the triplet energy:

$$-h\sum_i \sigma_i - J_3 \sum_{<i,j,k>} \sigma_i\sigma_j\sigma_k$$
$$= -h\left(\sum_{\alpha-sites} \sigma_\alpha + \sum_{\beta-sites} \sigma_\beta + \sum_{\gamma-sites} \sigma_\gamma\right)$$

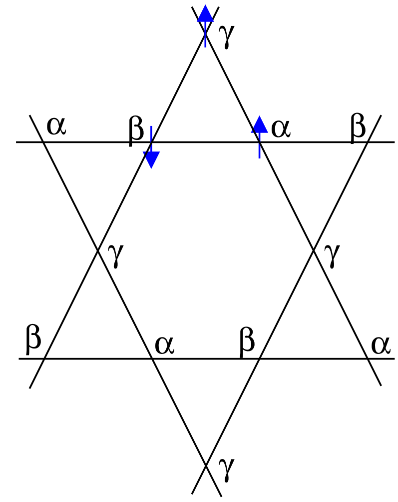

FIG. 5. Three-sublattice decomposition of a kagomé lattice, showing one of the six possible ground states of a frustrated elementary triangle.

$$-J_3 \sum_{<\alpha,\beta,\gamma>} \sigma_\alpha\sigma_\beta\sigma_\gamma$$
$$= -\left[h\left(\frac{N}{3} - \frac{N}{3} + \frac{N}{3}\right) + J_3\left(-\frac{2}{3}N\right)\right]$$
$$= 0, \quad \text{if} \quad h = 2J_3. \quad (5.3)$$

Thus at $h = 2J_3$, the Zeeman and the triplet energies cancel exactly.

It then follows that all exactly known ground-state results in the one-parameter kagomé Ising antiferromagnet can also be ascribed to the ground state of the current three-parameter model. For example, the internal energy $\mathcal{U}$ for the one-parameter model H^1_k is obtained by

$$H^1_k = -J_2 \sum_{\langle i,j\rangle} \sigma_i\sigma_j, \quad J_2 < 0,$$
$$\mathcal{U} = \langle H^1_k\rangle = -J_2\left(\frac{N \times 4}{2}\right)\langle\sigma_0\sigma_1\rangle. \quad (5.4)$$

The nearest-neighbor pair correlation $\langle\sigma_0\sigma_1\rangle$ is known [77] as a function of temperature, which has the value $-1/3$ at zero temperature. So, using (5.4), the ground-state binding energy becomes

$$\mathcal{U}_0 = E_0 = \frac{2}{3}NJ_2, \quad J_2 < 0. \quad (5.5)$$

The residual entropy S_0, given a ground-state degeneracy W_0, is obtained by the Boltzmann formula $S_0 = k_B \ln W_0 = Nk_B \ln w_0 = Nk_B \times 0.50183\ldots$, using exact results from [58]. Thus, for $\ln w_0 \approx 1/2$, the number of degenerate states is approximately $W_0 \approx e^{N/2}$, where $N = N_A = 6 \times 10^{23}$ is the Avogadro number. This extremely large degeneracy is *accidental* and hence cannot be lifted by "spontaneous symmetry breaking." These ground-state properties remain valid for our three-parameter model (2.2) in the $L^* = 0$ subspace, although the excitations will be very different.

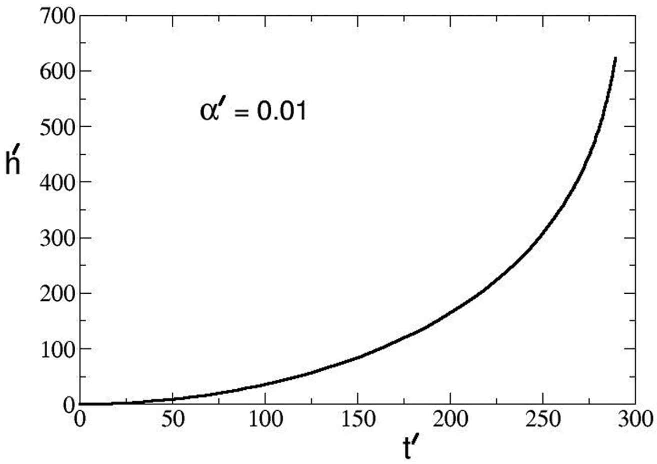

FIG. 6. Dimensionless field $h' = h/2|J_2|$ as a function of the dimensionless temperature $t' = k_BT/2|J_2|$ for $\alpha'(\equiv -J_3/J_2) = 0.01$, showing that the two are no longer independent under the $L^* = 0$ condition. The $L^* = 0$ crossover temperature from FD to NFD is $t'_{\rm cross} \approx 297.3$.

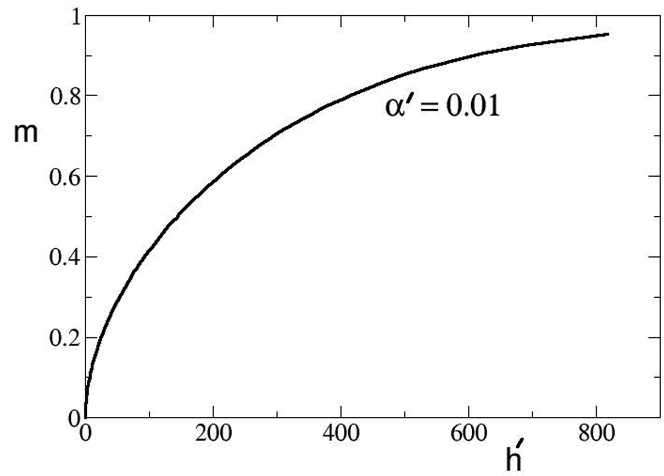

FIG. 7. Induced magnetization m as a function of the dimensionless field $h' = h/2|J_2|$ for $\alpha' = 0.01$, where $\alpha' \equiv -J_3/J_2$. Note that since h' is a function of dimensionless temperature t', each point on the curve corresponds to a different temperature, as obtained from Fig. 6.

B. Magnetization

We will define a dimensionless temperature t' and a dimensionless field h' as

$$t' \equiv \frac{k_BT}{2|J_2|}, \quad h' \equiv \frac{h}{2|J_2|}. \tag{5.6}$$

In addition, since the ground-state phase boundary is symmetric in J_3, we will consider $J_3 > 0$ only.

The magnetization m is simply related to the density ρ in the fluid representation by the correspondence relation $m = 2\rho - 1$, where the density, evaluated at $L^* = 0$, is given by (see [76])

$$\rho_{L^*=0} = \frac{2}{3}z\frac{\partial \ln a^*}{\partial z} + (\langle\mu_0\mu_1\rangle - \tanh K^*)z\frac{\partial K^*}{\partial z}. \tag{5.7}$$

Here a^* appears in (3.14), and $\langle\mu_0\mu_1\rangle$, to be evaluated at $L^* = 0$, is the nearest-neighbor pair correlation which is known exactly in terms of complete elliptic integrals. Note that in the NFD region $K^* > 0$, so $\langle\mu_0\mu_1\rangle$ is positive, while in the FD region $K^* < 0$, so $\langle\mu_0\mu_1\rangle$ is negative. The logarithmic derivative of a^* in (5.7) has been worked out in the Appendix of [76]. Using these results, we can find the magnetization m as a function of the temperature.

The important point to keep in mind is that within the $L^* = 0$ subspace, the condition imposed by the cubic algebraic equation for the fugacity implies that the chemical potential and the temperature in the fluid representation are no longer independent variables. In the magnetic representation, this implies that the field h' and the temperature t' are not independent on this subspace. Figure 6 shows $h'(t')$ due to the imposed $L^* = 0$ condition, for a particular value $\alpha' = 0.01$. Thus the magnetization m is no longer a function of two independent variables h' and t'. In particular, magnetization as a function of temperature alone is not a physically observable function since the field itself changes with temperature, which in turn affects the magnetization. On the other hand, since both magnetization $m(t')$ and the field $h(t')$ are functions of temperature, the magnetization $m(h(t'))$ as a functional of the field $h(t')$, plotted for each given temperature t', should remain a physically observable function. Figure 7 shows magnetization as a function of the dimensionless field h' for $\alpha' = 0.01$; this should offer insights into the magnetic properties of a standard kagomé Ising antiferromagnet ($\alpha' \to 0$) in the presence of a field. For larger values of α', the magnetization rises faster to full magnetization $m = 1$ as shown in Fig. 8. It also shows a clear threshold at $h'_{th} = \alpha'$ below which the magnetization is zero, consistent with (4.4). Note that this threshold value is an exact zero-temperature property.

The existence of the threshold has important consequences. The fact that the magnetization does not change until the external applied field h reaches a certain threshold value ($h = 2J_3$) implies that the spectrum is gapped, the gap tending to zero as $J_3 \to 0$. The magnetization starts to increase with

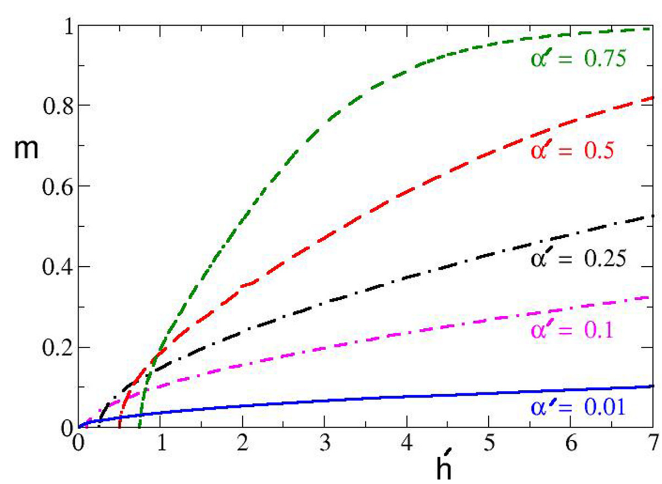

FIG. 8. Induced magnetization m as a function of the dimensionless field $h' = h/2|J_2|$ for different values of α', showing the exact threshold at $h'_{th} = \alpha'$. The parameter α' is defined as $\alpha' \equiv -J_3/J_2$.

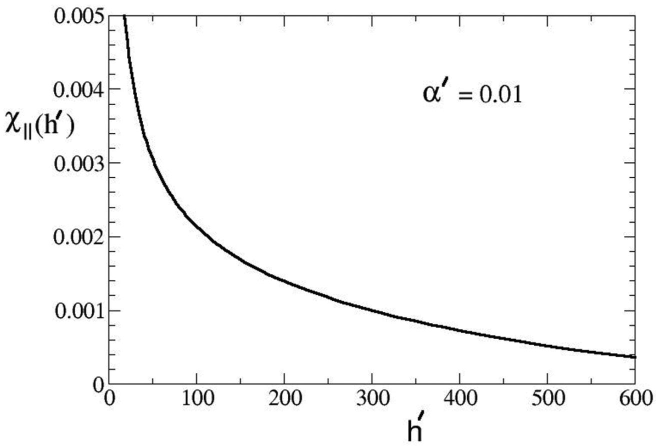

FIG. 9. Parallel magnetic susceptibility $\chi_{\|}(h') = \partial m/\partial h'$ as a function of the dimensionless field $h' = h/2|J_2|$ for $\alpha' = 0.01$, where $\alpha' \equiv -J_3/J_2$. Note that h' itself is a function of temperature in the $L^* = 0$ subspace, so this is not an isothermal susceptibility.

an infinite slope beyond the threshold value, resulting in a divergence of the parallel susceptibility at zero temperature (discussed next).

C. Magnetic susceptibility

Given the magetization vs field plot shown in Fig. 8, it is possible to numerically evaluate the derivative and obtain the parallel magnetic susceptibility as a function of the dimensionless field h' defined in (5.6). Figure 9 shows the parallel magnetic susceptibility $\chi_{\|}(h') = \partial m/\partial h'$ as a function of the dimensionless field h' for $\alpha' = 0.01$. The susceptibility diverges at the threshold value $h' = \alpha'$, showing that in the plot m vs h' in Fig. 8, the magnetization m hits the h' axis with a perpendicular slope at zero temperature. Since both the magnetization and the field are functions of temperature in the $L^* = 0$ subspace, we can obtain the temperature-dependent parallel susceptibility by considering $\frac{\partial m(t')}{\partial h'(t')} = \frac{\partial m/\partial t'}{\partial h'/\partial t'}$. Figure 10 shows the susceptibility $\chi_{\|}(t')$ for $\alpha' = 0.01$.

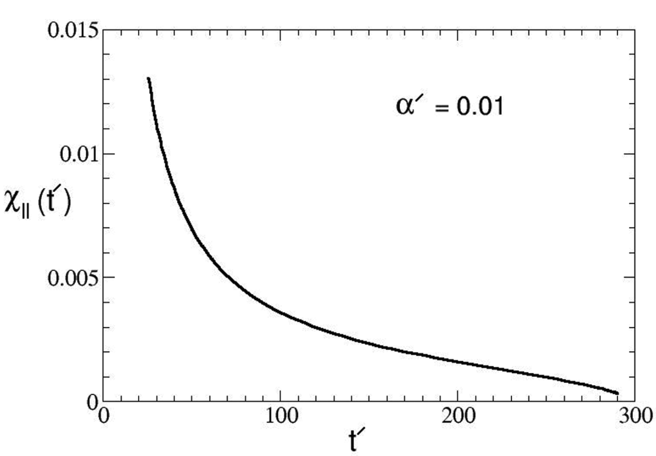

FIG. 10. Parallel magnetic susceptibility $\chi_{\|}(t') = \frac{\partial m(t')}{\partial h(t')} = \frac{\partial m/\partial t'}{\partial h/\partial t'}$ as a function of the dimensionless temperature $t' = k_B T/2|J_2|$ for $\alpha' = 0.01$ ($\alpha' \equiv -J_3/J_2$).

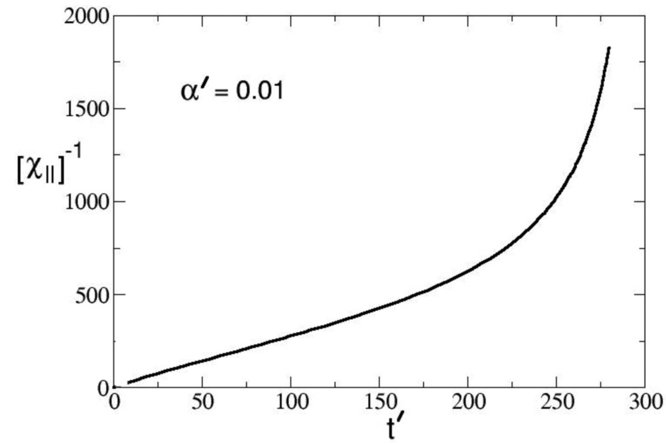

FIG. 11. Inverse parallel magnetic susceptibility $[\chi_{\|}(t')]^{-1}$ as a function of dimensionless temperature $t' = k_B T/2|J_2|$ for $\alpha' = 0.01$ ($\alpha' \equiv -J_3/J_2$). The $L^* = 0$ crossover temperature for $\alpha' = 0.01$ is $t'_{\text{cross}} \approx 297$. (See higher resolution near origin in accompanying Fig. 12.)

Note that the highest temperature is limited by the $L^* = 0$ crossover boundary T_{cross} between FD and NFD, shown in Fig. 4. Defining

$$t'_{\text{cross}} = \frac{k_B T_{\text{cross}}}{2|J_2|}, \tag{5.8}$$

the crossover temperature at $\alpha' = 0.01$ is $t'_{\text{cross}} \approx 297$. This is reflected in the divergence of the field at that temperature in Fig. 6.

While the high-temperature behavior is complicated by the FD-NFD crossover boundary, the susceptibility shows a Curie-Weiss behavior at temperatures well below the $L^* = 0$ crossover temperature, of the form $1/(T + T_0)$, T_0 being a constant. This is more clearly visible if we plot the inverse susceptibility $[\chi_{\|}(t')]^{-1}$, which is linear in T but with a finite positive value at $T = 0$. Figure 11 shows the inverse susceptibility for $\alpha' = 0.01$.

Figure 12 shows a rough straight line interpolation from "high" (but well below the $L^* = 0$ crossover) temperature giving a Curie-Weiss temperature $\Theta_{CW} \approx 2$ in units of $2|J_2|/k_B$. This should be compared with the predicted value [59] $\Theta_{CW}^{KIA} = 2$ for the kagomé Ising antiferromagnet ($\alpha' \to 0$). We emphasize that unlike a standard antiferromagnet, the range of linear temperature exists only to an intermediate extent, the high-temperature part clearly deviating from a linear behavior due to the existence of the crossover boundary beyond which there is no frustration. Moreover, as α' is increased, the $L^* = 0$ crossover temperature decreases and the range over which the inverse susceptibility is linear becomes progressively smaller. For example, for $\alpha' = 0.1$, 0.25, 0.5 and 0.75, the $L^* = 0$ crossover temperature is $t'_{\text{cross}} \approx 27.34$, 9.35, 3.34, and 1.28, respectively. Thus estimating Θ_{CW} as a function of α' from a fitting of the small linear temperature range becomes unreliable. Nevertheless, even though no attempt was made to obtain an accurate estimate of the magnitude of Θ_{CW}, a trend was seen for $\alpha' \ll 1$, namely, that the value of Θ_{CW} decreases

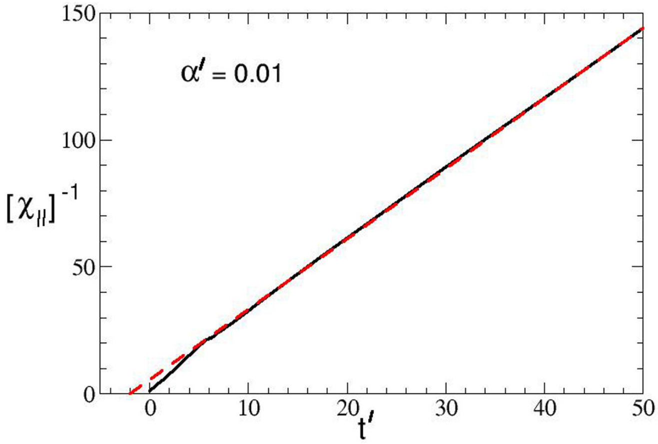

FIG. 12. Inverse parallel magnetic susceptibility $[\chi_\parallel(t')]^{-1}$ as a function of dimensionless temperature $t' = k_BT/2|J_2|$ for $\alpha' = 0.01$ ($\alpha' \equiv -J_3/J_2$), showing a rough linear fit (red dashed line) up to $t' = 50$ (well below the $L^* = 0$ crossover temperature $t'_{\rm cross} \approx 297$), leading to an approximate Curie-Weiss temperature $\Theta_{CW} \approx 2$ in units of $2|J_2|/k_B$.

as α' increases. For example, Fig. 13 shows the result for $\alpha' = 0.1$, where $\Theta_{CW}(\alpha' = 0.1)$ is found to be smaller than $\Theta_{CW}(\alpha' = 0.01)$ shown in Fig. 12.

VI. FRUSTRATED DISORDER BEYOND $L^* = 0$

The term L^* in (3.13) can be considered as an effective one-particle potential that depends not only on the parameters h, J_2, and J_3 of the original Hamiltonian (2.2) but also on temperature T. The results presented above are valid in the $L^* = 0$ subspace where the field h is not an independent parameter but is tuned to satisfy the $L^* = 0$ condition. In this section we study the possibility if the solutions for $L^* = 0$ can be used to explore the region $L^* \neq 0$. We show that a *hybrid variable u*, defined in terms of the fluid parameters as $u \equiv x^2 z$, plays an important role beyond the $L^* = 0$ subspace.

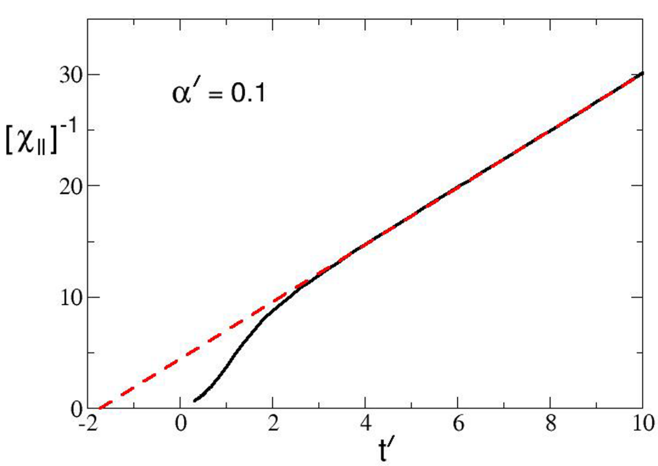

FIG. 13. Inverse parallel magnetic susceptibility $[\chi_\parallel(t')]^{-1}$ as a function of dimensionless temperature $t' = k_BT/2|J_2|$ for $\alpha' = 0.1$ ($\alpha' \equiv -J_3/J_2$). A rough linear fit (red dashed line) up to $t' = 10$ (well below the $L^* = 0$ crossover temperature $t'_{\rm cross} \approx 27$) leads to an approximate Curie-Weiss temperature $\Theta_{CW} < 2$ in units of $2|J_2|/k_B$.

We first rewrite u in terms of the magnetic parameters:

$$u \equiv x^2 z = e^{2\beta\epsilon_2(1+\frac{\mu}{2\epsilon_2})}. \tag{6.1}$$

Correspondence relations (3.11) and (3.12) give

$$\frac{\mu}{\epsilon_2} = \frac{1}{1+\alpha'}\left[\frac{h}{2J_2} - 2 - \alpha'\right]. \tag{6.2}$$

Thus

$$\ln u = 2\beta\epsilon_2\left(1 + \frac{\mu}{2\epsilon_2}\right) = \frac{\beta\epsilon_2}{(1+\alpha')}\frac{1}{2J_2}(h - 2J_3). \tag{6.3}$$

Now use $K_2/4 = K - M$ from (3.5) to obtain

$$\beta\epsilon_2 = 4\beta J_2(1+\alpha'), \tag{6.4}$$

which finally gives

$$u \equiv x^2 z = e^{2(h-2J_3)/k_BT}. \tag{6.5}$$

Thus $h = 2J_3$, which corresponds to $L^* = 0$ at zero temperature, is equivalent to $u = 1$. Only for this value of u, V/U in (D3) is zero, consistent with $L^* = 0$. Note that (6.4) can be used to write x in terms of magnetic variables, $x \equiv e^{-|\epsilon_2|/k_BT} = e^{-4|J_2-J_3|/k_BT}$.

The honeycomb "dressed" parameters L^* and K^* are clearly interrelated. It turns out that in the low-temperature region both K^* [given by (3.16)] and $f = \tan\theta$ [given by (A7)], where $L^* = i\theta$, become functions of the single variable u:

$$\begin{aligned} K^*(x^{1-\alpha} \ll 1) &= \frac{1}{4}\ln\left[1 - \frac{3u}{(u+1)^2}\right], \\ \tan\theta(x \ll 1) &= \frac{1-2u+s}{1+s}\sqrt{\frac{1+u+s}{1+u-s}}, \\ s &\equiv \sqrt{1-u+u^2}. \end{aligned} \tag{6.6}$$

It is then possible to obtain a direct relationship between K^* and θ at low temperatures by eliminating u. Figure 14(a) exhibits such a relationship evidencing a parabolic minimum at $\theta = 0$, $K^* = K^*_{min} = -\frac{1}{2}\ln 2 = -0.3465\ldots$ (see Fig. 2), and showing symmetric side-wings with tips at $\theta = \pm\pi/2 = \pm 1.5707\ldots$ radians. For comparison, we also show the low-temperature expressions for K^* vs u and $\tan\theta$ vs u using (6.6). The region around the minimum of K^* near $\theta = 0$ in Fig. 14(a) corresponds to $|u-1| \ll 1$.

The hybrid variable u thus offers a possible approach to the region $L^* \neq 0$, starting from the known results for $L^* = 0$ which defines a subspace $h(T)$ given in (C7) for $x \ll 1$. Figure 14(c) suggests that for small deviation from $L^* = i\theta = 0$ in the region $x \ll 1$, we expand $\tan\theta \approx \theta$ around $u = 1$. Using (6.6) this gives $\theta \approx (-3\sqrt{3}/4)(u-1)$ or $u \approx e^{-4\theta/3\sqrt{3}}$. Comparing with (6.5), this implies that we tune the field h such that

$$h = 2J_3 - \frac{2k_BT}{3\sqrt{3}}\theta; \quad u = e^{-\frac{4}{3\sqrt{3}}\theta}, \quad x \ll 1, \quad |\theta| \ll 1. \tag{6.7}$$

This defines a subspace $h(T)$ for $L^* \neq 0$, which coincides with the $L^* = 0$ subspace as $T \to 0$. Experiments in the laboratory can probe such subspaces by sweeping either the magnetic

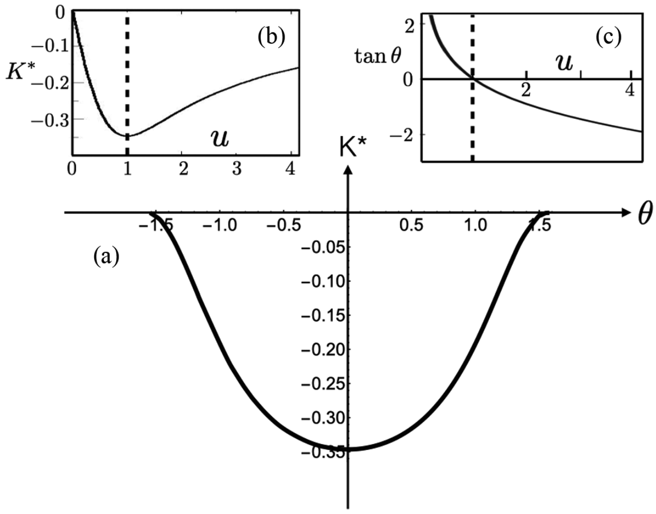

FIG. 14. (a) K^* vs θ (radians), where $L^* = i\theta$, in the FD domain and low-temperature region $x \ll 1$. The ground state corresponds to the bottom of the well with $L^* = 0$, i.e., $\theta = 0$. The region near the bottom of the well corresponds to a magnetic field h such that $2|h - 2J_3| \ll k_B T$. In terms of the hybrid variable $u = e^{2(h-2J_3)/k_B T}$, this corresponds to $|u - 1| \ll 1$. Panels (b) and (c) show K^* and $\tan\theta$ vs u, respectively, where the dashed lines correspond to $u = 1$.

field h or temperature T or both, always satisfying (6.7). It should therefore be possible to obtain insights into the $L^* \neq 0$ region by developing a perturbation theory around $L^* = 0$, the minimum of K^*, with $|\theta| \ll 1$ as the small parameter.

As discussed earlier, $L^* = 0$ is a condition among the three parameters J_2, J_3, and h in (2.2) so that only two of them can be varied independently. In other words, it defines a two-parameter surface in the three-dimensional space spanned by the three parameters. Figure 3(c) shows an example of such a surface at zero temperature. In Sec. V we obtained accurate results for magnetization and susceptibility for the three-parameter model (2.2), but valid only for points on the particular surface defined by the condition $L^* = 0$. The discussion above shows that it should be possible to extend those results to other points beyond the $L^* = 0$ surface, albeit only within a perturbation theory valid for points close to the $L^* = 0$ surface.

VII. SUMMARY AND DISCUSSION

The exact solutions for an Ising antiferromagnet on a kagomé lattice with either purely nearest-neighbor pair interactions or purely triplet interactions as given in (2.1) are known separately. They provide insights about the role of geometrical frustration vs nonfrustrated disorder in the destruction of long-range order in classical spin systems. In this work, we solve an Ising model when both pair and triplet interactions are combined, exploring the interplay of disorder with and without frustration. The mathematical trick we use is to add a magnetic field, making it apparently a more difficult three-parameter model; but this allows an exact mapping on to a standard honeycomb Ising model with pair interaction K^* and a finite field L^*, with no triplet interaction. The mapping is via a lattice-gas model in a grand canonical ensemble in which the chemical potential relates to the magnetic field. While the general three-parameter kagomé Ising antiferromagnetic model remains unsolvable for magnetization and magnetic susceptibility, it develops that solutions can be determined on a two-parameter subspace, given by the condition $L^* = 0$.

Within the two-parameter subspace, a projection of the finite temperature results on to zero temperature J_2-J_3 plane allows us to obtain the exact zero-temperature phase diagram shown in Fig. 3(b). It shows that the disordered phase has two distinct regions. The horizontally shaded regions in Fig. 3(b) correspond to nonfrustrated disorder (NFD), because the pair interaction K^* in the standard Ising model on the associated honeycomb lattice is positive (ferromagnetic). On the other hand, the vertically shaded region corresponds to frustrated disorder (FD), with $K^* < 0$. We expect the magnetic properties of these two regions to be qualitatively different, since all zero-field odd-number spin-correlations must vanish for $K^* < 0$ as shown in Appendix B. Indeed, as shown in [59], the perpendicular susceptibility $\chi_\perp$ on the line $J_3 = 0$, $J_2 < 0$, which belongs to the FD region, diverges as $T \to 0$ while $\chi_\perp$ remains finite along the line $J_2 = 0$, which belongs to the NFD regime.

It turns out that the $L^* = 0$ condition also allows exact solutions for magnetization and parallel magnetic susceptibility on the two-parameter subspace. The magnetization as a function of the field h shows a threshold at $h = 2J_3$, which implies a gapped spectrum for the three-parameter model. The parallel magnetic susceptibility shows the expected Curie-Weiss behavior. Note that the $\alpha' \to 0$ limit corresponds to the “pure” ($J_3 = 0$) kagomé Ising antiferromagnet in a field.

While we restrict our calculations to the $L^* = 0$ subspace only, we argue that the results beyond the subspace should be qualitatively similar when L^* is a small perturbation. In particular, the ground-state phase diagrams as well as the existence of a gapped spectrum in the presence of J_3 should remain valid. We argue that it should be possible to develop a systematic perturbation theory around $L^* = 0$ in terms of the hybrid variable $u = e^{2(h-2J_3)/k_B T}$ with $|u - 1| \ll 1$.

As mentioned in the Introduction, triplet interactions in geometrically frustrated systems are not ubiquitous, although they might be present as a small perturbation to a dominant pair interaction. Unfortunately, the crossover from FD to NFD at zero temperature happens only at triplet interactions that are equal in magnitude to the pair interaction. However, we also find that a disordered system which is geometrically frustrated at zero temperature can become nonfrustrated at some higher temperature, given in Fig. 4. For the pure pair interaction this happens only at $T \to \infty$, but in a system with a small but finite J_3 the crossover temperature could be experimentally accessible.

We have considered the addition of triplet interactions because a kagomé magnet with solely triplet interactions leads to a nonfrustrated disordered ground state [59]. We expect that any other model that leads to a similar ground state (perhaps including long-range interactions like RKKY; see, e.g., [81]) should lead to a similar phase diagram when added to the kagomé antiferromagnet with pair interactions. Our exact results should provide insights and guidance into the role of frustration in such models as well.

APPENDIX A: GEOMETRICAL FRUSTRATION AND PURE IMAGINARY L^*

The expressions for L^* and a^* in (3.14), as given in [76], are

$$\tanh L^* = \frac{V}{U}\left(\frac{\delta - A + C}{\delta + A - C}\right)^{1/2},$$
$$e^{2K^*} = \frac{\delta}{|C-A|}, \quad a^* = \frac{FU}{B(1+\eta^2)^{3/2}}, \tag{A1}$$
$$A = c^2 - bd, \quad B = ad - bc, \quad C = ac - b^2,$$
$$\eta = -\frac{A+C}{B} + \frac{\delta}{B}\mathrm{sgn}(C-A),$$
$$\delta = [(A+C)^2 + B^2]^{\frac{1}{2}}, \quad F = \eta(B\eta + 2C), \tag{A2}$$
$$U = (b+d)\eta + a + c,$$
$$V = (a+c)\eta - (b+d),$$

the vertex weights a, b, c, d being

$$a = x^3yz^{3/2}, \quad b = xz, \quad c = \sqrt{z}, \quad d = 1, \tag{A3}$$

where x, y, and z are defined in (3.8).

The sign of the quantity $C - A$ is important as it appears in the expression for $\tanh L^*$. We have

$$C - A = ac - b^2 - c^2 + bd = z[(xy-1)x^2z - 1 + x] \tag{A4}$$

with $y = x^{-\alpha}$. The sign of $C - A$ is known to be positive for ferromagnetic interaction $K^* > 0$, as shown in [76]. For the present case of antiferromagnetic interaction $K^* < 0$, in the zero-temperature limit $x \to 0$ and for $\alpha < 1$ in the FD region, we get $C - A \to z[-x^2z - 1] < 0$, which agrees with the Wu theory [80]. Then the expression for L^* can be written as

$$\tanh L^* = \frac{V}{U}\left(\frac{e^{2K^*}+1}{e^{2K^*}-1}\right)^{1/2}. \tag{A5}$$

For $K^* < 0$ and finite, $0 < e^{2K^*} < 1$ and the square root is pure imaginary. Thus one can write

$$L^* = \mathrm{arctanh}\, i f = i \arctan f \equiv i\theta, \tag{A6}$$

yielding $f = \tan\theta$, where

$$f \equiv \frac{V}{U}\left(\frac{1+e^{2K^*}}{1-e^{2K^*}}\right)^{1/2}. \tag{A7}$$

APPENDIX B: GEOMETRICAL FRUSTRATION AND VANISHING OF ODD-NUMBER CORRELATIONS IN THE ASSOCIATED HONEYCOMB ISING MODEL

As shown in Appendix A, $L^* = i\theta$ is pure imaginary in FD domain: $K^*_{min} \leqslant K^* < 0$, $K^*_{min} = -\frac{1}{2}\ln 2$. We then have (here K^*_- means K^* in the FD domain)

$$Z^*(L^*, K^*) = Z^*(i\theta, K^*_-) = \sum_{\{\mu_l\}} e^{K^*_- \sum_{<i,j>}\mu_i\mu_j + i\theta\sum_k \mu_k}, \tag{B1}$$

$$e^{i\theta\mu_l} = \cos\theta + i(\sin\theta)\mu_l, \; \mu_l = \pm 1$$
$$= (\cos\theta)[1 + i(\tan\theta)\mu_l], \tag{B2}$$

$$e^{i\theta\sum_k \mu_k} = \prod_{k=1}^{\mathcal{N}^*} e^{i\theta\mu_k} = (\cos\theta)^{\mathcal{N}^*}\{[1 + i(\tan\theta)\mu_1]$$
$$\times [1 + i(\tan\theta)\mu_2]\cdots[1 + i(\tan\theta)\mu_{\mathcal{N}^*}]\}$$
$$= (\cos\theta)^{\mathcal{N}^*}\{1 - (\tan\theta)^2 \sum_{pairs} \mu_i\mu_j + (\tan\theta)^4$$
$$\times \sum_{quartets} \mu_i\mu_j\mu_k\mu_l + +i[(\tan\theta)\sum_i \mu_i \cdots$$
$$-(\tan\theta)^3 \sum_{triplets} \mu_i\mu_j\mu_k + \cdots]\}. \tag{B3}$$

Therefore, using (3.4) and (3.14),

$$e^{(L-2K+2M/3)\mathcal{N}} Z(L, K, M)$$
$$= (a^*/2)^{\mathcal{N}^*}(\cosh K^*_-)^{-3\mathcal{N}^*/2}$$
$$\times \sum_{\{\mu_l\}} e^{K^*_- \sum_{<i,j>}\mu_i\mu_j}\{1 - (\tan\theta)^2 \sum_{pairs}\mu_i\mu_j + \cdots$$
$$+ i[(\tan\theta)\sum_i \mu_i - \cdots]\}. \tag{B4}$$

Aside from the real prefactor, the imaginary contribution from the latter expression may be written as

$$i\sum_{\{\mu_l\}} e^{K^*_- \sum_{<i,j>}\mu_i\mu_j}\Bigg[(\tan\theta)\sum_i \mu_i - (\tan\theta)^3$$
$$\times \sum_{triplets}\mu_i\mu_j\mu_k + \cdots\Bigg] = iZ^*(0, K^*_-)\Bigg[(\tan\theta)\sum_i \langle\mu_i\rangle_0$$
$$-(\tan\theta)^3 \sum_{triplets}\langle\mu_i\mu_j\mu_k\rangle_0 + \cdots\Bigg]. \tag{B5}$$

The subscript 0 on thermal averages indicates their evaluation at $\theta = 0$, i.e., in the ground state ($T = 0$) of FD region (see Fig. 14). Since $Z(L, K, M)$ itself is manifestly real, the r.h.s. imaginary contribution must vanish, i.e., all above odd-number correlations vanish identically, the latter being a well-known criterion for disordered Ising systems having only even-number interactions.

APPENDIX C: FD: THE $L^* = 0$ SUBSPACE AS $T \to 0$

In the ferromagnetic case as shown in [76], $L^* = 0$ is a necessary condition for long-range order. In the present case there is no long-range order, and in addition L^* is pure imaginary (see Appendix A). Nevertheless, the condition $L^* = 0$ still leads to the same cubic equation for the fugacity z as in the ferromagnetic case [76],

$$z^3 + a_2z^2 + a_1z + a_0 = 0, \tag{C1a}$$

with real coefficients

$$a_2 = \frac{3(x^2y - 2xy + 1)}{x^3y(x^3y^2 - 3xy + 2)}, \tag{C1b}$$

$$a_1 = -\frac{3(x^2y - 2x + 1)}{x^5y(x^3y^2 - 3xy + 2)}, \tag{C1c}$$

$$a_0 = -\frac{(x^3y - 3x + 2)}{x^6y(x^3y^2 - 3xy + 2)}. \tag{C1d}$$

This defines a two-parameter subspace in the three-parameter space of (x, y, z), or equivalently $(\mu, \epsilon_2, \epsilon_3)$.

Using the relation $y = x^{-\alpha}$, the real solution of the cubic equation depends on the parameter α. In the frustrated regime where $\alpha < 1$, the discriminant

$$D = Q^3 + R^2 < 0, \tag{C2}$$

with $Q \equiv (3a_1 - a_2^2)/9$, $R \equiv (9a_1a_2 - 27a_0 - 2a_2^3)/54$. While there are three inequivalent real solutions, the one *positive* solution is given by

$$\begin{aligned} z &= (R + \sqrt{D})^{1/3} + (R - \sqrt{D})^{1/3} - \frac{a_2}{3} \\ &= 2\sqrt{-Q}\cos\left(\frac{\pi - \phi}{3}\right) - \frac{a_2}{3}, \end{aligned} \tag{C3}$$

with $\cos\phi = -R/\sqrt{-Q^3}$. This defines a relationship among the fluid parameters x, y, and z due to the added condition $L^* = 0$. As $T \to 0$, or equivalently $x \to 0$,

$$\begin{aligned} &\phi \to \sqrt{3}x^{1-\alpha}; \quad \cos\left(\frac{\pi - \phi}{3}\right) \to \frac{1}{2}(1 + x^{1-\alpha}), \\ &\sqrt{-Q} \to \frac{1}{2}\frac{1}{x^{3-\alpha}}\left(1 + \frac{1}{2}x^{1-\alpha}\right), \\ &a_2 \to \frac{3}{2}\frac{1}{x^{3-\alpha}}\left(1 - \frac{1}{2}x^{1-\alpha}\right). \end{aligned} \tag{C4}$$

Combining all, the fugacity (C3) becomes

$$z = \frac{1}{x^2}\left(1 + \frac{8}{3}x^{1-\alpha}\right) + \cdots, \quad x \ll 1, \tag{C5}$$

which is equivalent to

$$\frac{\mu}{|\epsilon_2|} = 2 + \frac{8}{3}\frac{k_BT}{|\epsilon_2|}e^{-(1-\alpha)|\epsilon_2|/k_BT} + \cdots, \quad x \ll 1. \tag{C6}$$

Using the fluid-magnet correspondence relations (3.11) and (3.12), this implies

$$\frac{h}{2J_3} = 1 + \frac{2}{3}\frac{k_BT}{J_3}e^{-4(1-\alpha')|J_2|/k_BT} + \cdots, \quad x \ll 1. \tag{C7}$$

In the zero-temperature limit, $z \to \frac{1}{x^2}$, $x \to 0$,

$$x^2z \to 1, \quad \frac{\mu}{|\epsilon_2|} \to 2, \quad \frac{h}{2J_3} \to 1, \quad \text{as} \quad T \to 0. \tag{C8}$$

APPENDIX D: LIMITS $L^*(T \to 0)$: FD vs NFD

As seen from (A7), for any $K^* \neq 0$, whether L^* is zero or not will depend on the ratio V/U. Using definitions of (A1)–(A3), and for $1 < \alpha < 3$, one obtains $C - A > 0$ and

$$\frac{V}{U} = \frac{\eta\gamma - 1}{\eta + \gamma}, \quad \gamma = \frac{a + c}{b + d}. \tag{D1}$$

In the NFD region [see Fig. 3(a)], a finite K^*, given by (3.16), exists in the $T \to 0$ limit only if $w \equiv x^{3-\alpha}z$ remains finite. Then

$$\begin{aligned} &\eta(x \to 0) \to -\frac{1}{2}xz^{1/2}, \quad \gamma \to \frac{1 + w}{xz^{1/2}}, \\ &\frac{V}{U} \to -\frac{3 + w}{1 + w}xz^{1/2} \to 0, \quad \text{as} \quad T \to 0. \end{aligned} \tag{D2}$$

This implies that $L^* \to 0$ as $T \to 0$ for any finite w in this NFD region.

On the other hand for $\alpha < 1$, i.e., $C - A < 0$, a nontrivial finite (and negative) K^* exists in the zero-temperature limit only if the *hybrid variable* $u \equiv x^2z$ remains finite. In this FD region, as $T \to 0$,

$$\begin{aligned} &\eta(x \to 0) \to \frac{(1 - u) + \sqrt{1 - u + u^2}}{\sqrt{u}}, \quad \gamma \to \frac{1}{\sqrt{u}} \\ &\frac{V}{U} \to \frac{1 - 2u + \sqrt{1 - u + u^2}}{1 + \sqrt{1 - u + u^2}}, \end{aligned} \tag{D3}$$

where the latter ratio is zero only if $u = 1$.

[1] P. W. Anderson, Mater. Res. Bull. **8**, 153 (1973).
[2] A. P. Ramirez, Annu. Rev. Mater. Sci. **24**, 453 (1994).
[3] P. A. Lee, Science **321**, 1306 (2008).
[4] L. Balents, Nature (London) **464**, 199 (2010).
[5] C. Lacroix, P. Mendels, and F. Mila, *Introduction to Frustrated Magnetism* (Springer-Verlag, Berlin, 2011).
[6] H. T. Diep, *Frustrated Spin Systems*, 2nd ed. (World Scientific, Singapore, 2013).
[7] Y. Zhou, K. Kanoda, and T.-K. Ng, Rev. Mod. Phys. **89**, 025003 (2017).
[8] X. Obradors, A. Labarta, A. Isalgue, J. Tejada, J. Rodriguez, and M. Pernet, Solid State Commun. **65**, 189 (1988).
[9] A. P. Ramirez, G. P. Espinosa, and A. S. Cooper, Phys. Rev. Lett. **64**, 2070 (1990).
[10] M. J. Harris, S. T. Bramwell, D. F. McMorrow, T. Zeiske, and K. W. Godfrey, Phys. Rev. Lett. **79**, 2554 (1997).
[11] S. H. Lee, C. Broholm, W. Ratcliff, G. Gasparovic, Q. Huang, T. H. Kim, and S.-W. Cheong, Nature (London) **418**, 856 (2002).
[12] V. Fritsch, J. Hemberger, N. Büttgen, E.-W. Scheidt, H.-A. Krug von Nidda, A. Loidl, and V. Tsurkan, Phys. Rev. Lett. **92**, 116401 (2004).
[13] S. Nakatsuji, Y. Nambu, H. Tonomura, O. Sakai, S. Jonas, C. Broholm, H. Tsunetsugu, Y. Qiu, and Y. Maeno, Science **309**, 1697 (2005).
[14] T. Itou, A. Oyamada, S. Maegawa, M. Tamura, and R. Kato, Phys. Rev. B **77**, 104413 (2008).

[15] S. Yamashita, Y. Nakazawa, M. Oguni, Y. Oshima, H. Nojiri, Y. Shimizu, K. Miyagawa, and K. Kanoda, Nat. Phys. **4**, 459 (2008).
[16] T. Itou, A. Oyamada, S. Maegawa, and R. Kato, Nat. Phys. **6**, 673 (2010).
[17] Y. Furukawa, Science **350**, 631 (2015).
[18] M. Hirschberger, J. W. Krizan, R. J. Cava, and N. P. Ong, Science **348**, 106 (2015).
[19] M M. Hagihala, S. Hayashida, M. Avdeev, H. Manaka, H. Kikuchi, and T. Masuda, npj Quantum Mater. **4**, 14 (2019).
[20] K. Hofhuis, C. F. Petersen, M. Saccone, S. Dhuey, A. Kleibert, S. van Dijken, and A. Farhan, Phys. Rev. B **104**, 014409 (2021).
[21] P. Nikolic and T. Senthil, Phys. Rev. B **71**, 024401 (2005)
[22] J. Zheng and G. Sun, Phys. Rev. B **71**, 052408 (2005).
[23] A. S. Wills, R. Ballou and C. Lacroix, Phys. Rev. B **66**, 144407 (2002).
[24] T. Takagi and M. Mekata, J. Phys. Soc. Jpn. **62**, 3943 (1993).
[25] D. A. Huse and A. D. Rutenberg, Phys. Rev. B **45**, 7536 (1992).
[26] M. Wolf and K. D. Schotte, J. Phys. A: Math. Gen. **21**, 2195 (1988).
[27] H. Giacomini, J. Phys. A: Math. Gen. **21**, L31 (1988).
[28] R. Moessner, S. L. Sondhi, and P. Chandra, Phys. Rev. Lett. **84**, 4457 (2000).
[29] R. Moessner and S. L. Sondhi, Phys. Rev. B **63**, 224401 (2001).
[30] T. Balcerzak, K. Szalowski, M. Jascur, M. Zukovic, A. Bobak, and M. Borovsky, Phys. Rev. E **89**, 062140 (2014).
[31] D. Bergman, J. Alicea, E. Gull, S. Trebst, and L. Balents, Nat. Phys. **3**, 487 (2007).
[32] Y. Huh, M. Punk, and S. Sachdev, Phys. Rev. B **84**, 094419 (2011).
[33] E. Jurčišinová and M. Jurcisin, Phys. Rev. E **97**, 052129 (2018).
[34] P. W. Leung and V. Elser, Phys. Rev. B **47**, 5459 (1993).
[35] P. Lecheminant, B. Bernu, C. Lhuillier, L. Pierre, and P. Sindzingre, Phys. Rev. B **56**, 2521 (1997).
[36] C. Schröder, H. Nojiri, J. Schnack, P. Hage, M. Luban, and P. Kogerler, Phys. Rev. Lett. **94**, 017205 (2005).
[37] A. M. Läuchli, J. Sudan, and E. S. Sorensen, Phys. Rev. B **83**, 212401 (2011).
[38] H. C. Jiang, Z. Y. Weng, and D. N. Sheng, Phys. Rev. Lett. **101**, 117203 (2008).
[39] D. J. J. Farnell, R. F. Bishop, P. H. Y. Li, J. Richter, and C. E. Campbell, Phys. Rev. B **84**, 012403 (2011).
[40] A. F. Albuquerque, D. Schwandt, B. Hetenyi, S. Capponi, M. Mambrini, and A. M. Lauchli, Phys. Rev. B **84**, 024406 (2011).
[41] S. Yan, D. A. Huse, and S. R. White, Science **332**, 1173 (2011).
[42] L. Cano-Cortes, A. Ralko, C. Fevrier, J. Merino, and S. Fratini, Phys. Rev. B **84**, 155115 (2011).
[43] O. Rojas, S. M. de Souza, and N. S. Ananikian, Phys. Rev. E **85**, 061123 (2012).
[44] H. C. Jiang, Z. Weng, and L. Balents, Nat. Phys., **8**, 902 (2012).
[45] S. Depenbrock, I. P. McCulloch, and U. Schollwock, Phys. Rev. Lett. **109**, 067201 (2012).
[46] S. A. Kulagin, N. Prokofev, O. A. Starykh, B. Svistunov, and C. N. Varney, Phys. Rev. B **87**, 024407 (2013).
[47] O. Melchert and A. K. Hartmann, Phys. Rev. E **87**, 022107 (2013).
[48] Y. Iqbal, F. Becca, S. Sorella, and D. Poilblanc, Phys. Rev. B **87**, 060405(R) (2013).
[49] S. Nishimoto, N. Shibata, and C. Hotta, Nat. Commun. **4**, 2287 (2013).
[50] S. Yamaki, K. Seki, and Y. Ohta, Phys. Rev. B **87**, 125112 (2013).
[51] T. Yokota, Phys. Rev. E **89**, 012128 (2014).
[52] F. M. Zimmer, C. F. Silva, S. G. Magalhaes, and C. Lacroix, Phys. Rev. E **89**, 022120 (2014).
[53] M. Schmidt, C. V. Morais, and F. M. Zimmer, Phys. Rev. E **93**, 012147 (2016).
[54] H. J. Liao, Z. Y. Xie, J. Chen, Z. Y. Liu, H. D. Xie, R. Z. Huang, B. Normand, and T. Xiang, Phys. Rev. Lett. **118**, 137202 (2017).
[55] A. Andreanov and M. V. Fistul, Phys. Rev. B **102**, 140405(R) (2020).
[56] G. H. Wannier, Phys. Rev. **79**, 357 (1950).
[57] R. M. F. Houtappel, Physica (Amsterdam) **16**, 425 (1950).
[58] K. Kano and S. Naya, Prog. Theor. Phys. **10**, 158 (1953).
[59] K. A. Muttalib, M. Khatun, and J. H. Barry, Phys. Rev. B **96**, 184411 (2017).
[60] J. H. Barry and F. Y. Wu, Int. J. Mod. Phys. B **03**, 1247 (1989).
[61] C. Broholm, G. Aeppli, G. P. Espinosa, and A. S. Cooper, Phys. Rev. Lett. **65**, 3173 (1990).
[62] K. Matan, D. Grohol, D. G. Nocera, T. Yildirim, A. B. Harris, S. H. Lee, S. E. Nagler, and Y. S. Lee, Phys. Rev. Lett. **96**, 247201 (2006).
[63] M. Fu, T. Imai, T-H. Han, and Y. S. Lee, Science **350**, 655 (2015).
[64] Z. L. Dun, J. Trinh, K. Li, M. Lee, K. W. Chen, R. Baumbach, Y. F. Hu, Y. X. Wang, E. S. Choi, B. S. Shastry, A. P. Ramirez, and H. D. Zhou, Phys. Rev. Lett. **116**, 157201 (2016).
[65] M. W. Pestak, R. E. Goldstein, M. H. W. Chan, J. R. de Bruyn, D. A. Balzarini, and N. W. Ashcroft, Phys. Rev. B **36**, 599 (1987).
[66] B. M. Axilrod and E. Teller, J. Chem. Phys. **11**, 299 (1943).
[67] N. S. Sullivan, Bull. Magn. Reson. **11**, 86 (1987) and references cited therein.
[68] M. Roger, J. J. Hetherington, and J. M. Delrieu, Rev. Mod. Phys. **55**, 1 (1983).
[69] N. Yoshioka, Y. Akagi, and H. Katsura, Phys. Rev. E **99**, 032113 (2019).
[70] L. Berthier and G. Biroli, Rev. Mod. Phys. **83**, 587 (2011).
[71] V. Blum, G. L. W. Hart, M. J. Walorski, and A. Zunger, Phys. Rev. B **72**, 165113 (2005).
[72] G. Biroli and M. Mezard, Phys. Rev. Lett. **88**, 025501 (2001).
[73] J. K. Pachos and M. B. Plenio, Phys. Rev. Lett. **93**, 056402 (2004).
[74] C. D'Cruz and J. K. Pachos, Phys. Rev. A **72**, 043608 (2005).
[75] I. Bloch, J. Dalibard, and W. Zwerger, Rev. Mod. Phys. **80**, 885 (2008).
[76] J. H. Barry and K. A. Muttalib, Physica A **527**, 121326 (2019).
[77] J. H. Barry and M. Khatun, Int. J. Mod. Phys. B **11**, 93 (1997).
[78] C. M. Bender, Rep. Prog. Phys. **70**, 947 (2007).
[79] I. Syozi, in *Phase Transitions and Critical Phenomena*, edited by C. Domb and M. S. Green, Vol. 1 (Academic, New York, 1972).
[80] F. Y. Wu, J. Math. Phys. **15**, 687 (1974); X. N. Wu and F. Y. Wu, J. Stat. Phys. **50**, 41 (1988); K. Y. Lin and B. H. Chen, Int. J. Mod. Phys. B **04**, 123 (1990); X. N. Wu and F. Y. Wu, J. Phys. A: Math. Gen. **22**, L55 (1989); **22**, L1031 (1989); F. Y. Wu and X. N. Wu, Phys. Rev. Lett. **63**, 465 (1989); F. Y. Wu, J. Phys. A: Math. Gen. **23**, 375 (1990).
[81] C. Kittel, *Introduction to Solid State Physics*, 4th ed. (Wiley, Hoboken, NJ, 1971).